Biophysical Chemistry 22 (1985) 95–105
Elsevier

BPC 00928

PROPERTIES OF STRANGE ATTRACTORS IN YEAST GLYCOLYSIS

Mario MARKUS, Dietrich KUSCHMITZ and Benno HESS

Max-Planck-Institut für Ernährungsphysiologie, Rheinlanddamm 201, 4600 Dortmund 1, F.R.G.

Received 18th July 1984
Revised manuscript received 15th March 1985
Accepted 26th March 1985

Key words: Oscillation; Entrainment; Strange attractor; Chaos; Glycolysis; Biorhythm

The properties of periodic and aperiodic glycolytic oscillations observed in yeast extracts under sinusoidal glucose input were analyzed by the following methods. (1) Spectral analysis, rendering sharp peaks for periodic responses and enhanced broad-band noise for aperiodic oscillations. (2) Phase plane analysis, leading to closed and to open trajectories for periodic and aperiodic oscillations, respectively. (3) Rotation of a phase plane proportionally to time, revealing strange attractors associated with the aperiodic oscillations. (4) Stroboscopic plot on the phase plane, showing that the strange attractors follow a stretch-fold-press process, if the stroboscoping phase is varied. (5) Stroboscopic transfer plot, admitting a period of three transfer processes and thus implying chaos according to the Li-Yorke theorem. (6) Determination of the rate of information production by differentiation of the transfer plot, yielding approx. 0.21 bits per min for the chaotically glycolyzing yeast extract.

1. Introduction

Some time ago, oscillatory responses of yeast extracts [1,2] and yeast cells [3,4] upon application of a constant rate of substrate input were reported. Furthermore, entrainment of yeast extracts by the fundamental frequency, the 1/2-harmonic and the 1/3-harmonic of a sinusoidal source of substrate, were observed [5]. In an extension of our previous investigations [6,7], we posed the question as to whether more complex dynamic states, including chaotic oscillations, could be obtained in glycolysis under periodic excitation. Indeed, using an appropriate two-enzyme glycolytic model, we predicted a rich variety of periodic responses and strange attractors (deterministic chaos), which were recently confirmed experimentally in yeast extracts [8]. These measurements are subjected here to different evaluation techniques, obtaining clear evidence for chaos governed by deterministic laws ruling out random behaviour, and determining properties (shape and Liapunov characteristic exponent) of the strange attractors.

2. Experimental materials and methods

Experiments were performed with cell-free extracts of commercial baker's yeast (*Saccharomyces cerevisiae*) [3] (pH 6.4, 22–23°C, 20–27 mg protein/ml) by continuous and periodic injection of 0.3 M glucose and recording the NADH fluorescence (F) as given in ref. 8. The input flux rate was adjusted for each extract preparation, so that the period at constant input flux had a given standard value of approx. 12 min. All measurements of the fluorescence as a function of time were corrected by computer for a systematic linear drift. The value of the signal drift per min relative to the signal amplitude varied from experiment to experiment between 0 and 0.7%.

3. Techniques for the evaluation of the experiments

3.1. Power spectra analysis

The power spectrum [9] is given by:

$$P(\omega) = \frac{i}{\tau}\left|\int_0^{\tau} F(t)\, e^{-i\omega t}\, \mathrm{d}t\right|^2 \qquad (1)$$

where τ is the total measuring time. We obtained these spectra by an implemented fast Fourier transform using the subroutine FT01A from the Harwell Subroutine Library [10]. In this method, the number of evaluated points must be a power of two, so we used $2^{11} = 2048$ points from the measured curve. For periodic oscillations, the spectra are expected to show sharp peaks, while enhanced broad-band noise should signalize the randomness of aperiodic oscillations.

3.2. Phase plane plots

A phase space was constructed by introducing the derivative of the measured signal F, according to ref. 11. This treatment yields in the dF/dt–F plane closed curves for periodic oscillations, whereas chaotic oscillations are expected to fill up an attracting region randomly. The curves obtained by this method are plane projections of trajectories in the three-dimensional dF/dt–F–t space and thus an ever increasing number of curve intersections is expected for aperiodic oscillations, leading to confusing pictures when t becomes very large. Therefore, it is useful to introduce three-dimensional representations, as described in the next section.

3.3. Phase plane rotation

In order to obtain finite trajectories introducing time as a third dimension, we devised the following evaluation method: dF/dt is plotted vs. F on a plane and this plane is rotated around the dF/dt axis with angular velocity ω_e, where ω_e is the input flux frequency, so that one full rotation is completed after one input flux period $T_e = 2\pi/\omega_e$. The corresponding cartesian coordinates are: dF/dt, $F\cos(\omega_e t)$ and $F\sin(\omega_e t)$. For an entrained response with period mT_e, this display should lead to a curve closing after m full rotations, while an open trajectory filling up a strange attractor is expected for chaotic responses.

3.4. Stroboscopic plots on the phase plane

In order to visualize the folding properties of the strange attractors we used a display on the dF/dt–F plane at times equally spaced by the interval $\Delta t = T_e$ and at different phases, i.e., at times given by

$$t_n = (\varphi/360° + n)T_e, \quad n = 1, 2, \ldots, \tag{2}$$

where the phase φ should be dimensioned in degrees. This stroboscopic dF/dt–F plot is equivalent to a Poincaré map [12] of the trajectory described above (method of phase plane rotation) by intersecting this trajectory with a half plane defined by the angle φ.

3.5. Stroboscopic transfer functions

In this method, the signal F_{n+1} measured at the time t_{n+1} is plotted as a function of the signal F_n measured at t_n ($n = 1, 2, \ldots$), where the t_n are given by eq. 2. The choice of φ remains open. Setting $\varphi = 90°$ is equivalent to taking the t_n at the maxima of the input flux, as in ref. 8. Alternatively, we set here $\varphi = 0°$, thus plotting the signal at time $(n+1)T_e$ vs. the signal at time nT_e. The transfer function, computed by interpolation through the points obtained in this manner, permits us to obtain evidence for chaos by constructing a sequence having a period of three transfer processes. This allows the application of the theorem of Li and Yorke [13], which states that if a transfer function allows for such a sequence, then it allows for chaos.

3.6. Differentiation of the transfer function

We determined the Liapunov characteristic exponent by differentiating the curve obtained by interpolation of the stroboscopic transfer points (see section 3.5). This exponent is given by

$$\lambda = \lim_{n\to\infty} \frac{1}{n} \sum_{i=1}^{n} \log_2 \left|\frac{dy}{dx}\right|_i \tag{3}$$

for a transfer function $y = y(x)$ [14]. The single transfer processes are indexed by i. Chaos is characterized by $\lambda > 0$, while periodic oscillations are characterized by $\lambda < 0$. According to Oseledec's theorem [15], the value of λ given for a one-dimensional recurrence by eq. 3 is independent of our special choice of the transfer process in a

higher dimensional attractor. It can be shown (see ref. 14) that λ, as given by eq. 3, divided by the time taken for one transfer process is equal to the rate of information production expressed in bits per unit of time.

4. The model

The system is described by the following differential equations [6,7]:

$$\frac{d[F6P]}{dt} = \frac{d[PEP]}{dt} + \frac{d[ATP]}{dt} = \bar{V}_{in} + A \sin\omega_e t - V_{PFK} \quad (4)$$

$$\frac{d[ADP]}{dt} = -\frac{d[ATP]}{dt} = V_{PFK} - V_{PK} \quad (5)$$

where F6P is fructose 6-phosphate and PEP phospho*enol*pyruvate. $\bar{V}_{in}$ is the mean input flux. A and ω_e are the amplitude and the frequency of the periodic input flux. For periodic input flux, we set $A = \bar{V}_{in}$, a condition which is approximately met in the experiments. V_{PFK} and V_{PK} are the reaction rates of the enzymes phosphofructokinase (PFK) and pyruvate kinase (PK). V_{PFK} depends on [PEP], [ADP], [ATP] and [F6P] as given in ref. 16 under the additional assumption of random substrate binding with dissociation constants independent of the binding order. V_{PK} depends on [PEP], [ADP], [ATP], $[Mg^{2+}]$ and $[K^+]$ as given in ref. 17. $[Mg^{2+}]$ and $[K^+]$ (concentrations of unchelated cations) are determined from the total concentrations as described in ref. 18.

We normalized the fluxes by division through $V_{max(PK)}$ and the time by division through $K_{PEP}/V_{max(PK)}$, where $K_{PEP} = 0.31$ mM is a typical dissociation constant, namely, that of PEP with the R_1 state of PK (see ref. 17). Integrations of eqs. 4 and 5 were performed with the conditions given in ref. 7 using the subroutine DC01AD from the Harwell Subroutine Library [10].

5. Results

5.1. Comparison of theory and experiment

As a first step in the comparison between the theoretical predictions and experimental results, we described the system at constant input flux, by solving the differential eqs. 4 and 5 for $A = \omega_e = 0$. We thus obtained a limit cycle with a normalized frequency $\tilde{\omega}_0 = \omega_0 K_{PEP}/V_{max(PK)} = 0.13$ at a normalized mean input flux $\nu = \bar{V}_{in}/V_{max(PK)} = 0.12$. ω_0 is the non-normalized frequency of the limit cycle. Assuming $V_{max(PK)} = 1.4$ mM/min we obtain a period $T_0 = 2\pi/\omega_0 = 11$ min at $\bar{V}_{in} = 10$ mM/h. These values are comparable to those obtained from a typical experiment: $T_0 = 12$ min at $\bar{V}_{in} = 12$ mM/h.

Results of the calculations for a periodic input flux are given in fig. 1 as a basis for comparison of theory and experiment. The abscissa in fig. 1 covers a wide range of input frequencies ω_e, normalized with respect to the frequency ω_0 which is a constant. The ordinates of fig. 1 show values of [ADP] obtained at times nT_e, $n = 1, 2, \ldots$ (stroboscopic plot), while the abscissa is varied at a very slow rate, namely, at $\Delta\omega_e/\omega_0 = 1.2 \times 10^{-4}$ and 6.2×10^{-4} per input flux period in fig. 1a and b, respectively. As a consequence of the stroboscopic technique, m curves in a given interval of ω_e/ω_0 in fig. 1 indicate an oscillatory response with period $T = mT_e$, where $T_e = 2\pi/\omega_e$ is the period of the input flux. $m = 3$, for example, indicates entrainment by the 1/3-harmonic. Spread-out points in fig. 1 ($m \to \infty$) indicate chaos (letter C).

Fig. 1b is obtained by initiating the integration at $\omega_e/\omega_0 = 0.43$, [F6P] = 0.93 mM and [ADP] = 0.021 mM. Upon increasing ω_e/ω_0, fig. 1b shows a bifurcation from $m = 1$ to $m = 2$ at $\omega_e/\omega_0 = 1.4$. Further increase of ω_e/ω_0 leads to chaos via a period doubling cascade ($m = 2^n$) as described by Feigenbaum [19]. The chaotic region in the middle portion of fig. 1b shows a periodic window with $m = 5$ around $\omega_e/\omega_0 = 2.3$. Finally, we obtain $m = 3$ for $\omega_e/\omega_0 > 2.58$.

The fine structure of the middle portion of fig. 1b is shown in the expanded display in fig. 1a, which was obtained by starting the integration at $\omega_e/\omega_0 = 2.08$, [F6P] = 0.23 mM and [ADP] = 0.13 mM. Fig. 1a has a higher resolution than fig. 1b, owing to the slower rate of change of the abscissa value, thus revealing new narrower windows with different periods ($m = 6$, 7, etc.). Upon slowing down the rate of change of the abscissa even more (results not shown) an even higher resolution is

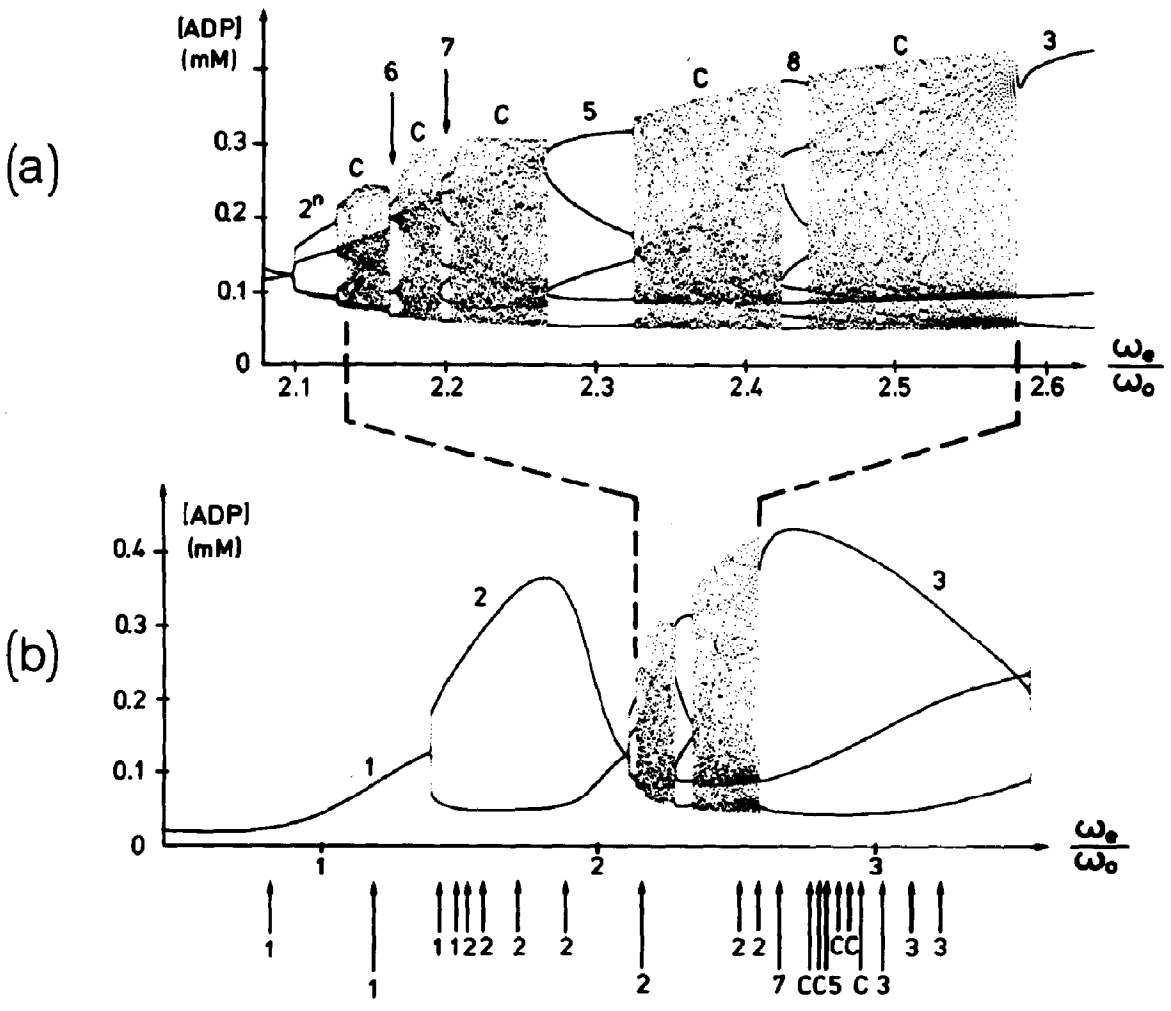

Fig. 1. ADP concentrations obtained stroboscopically under slow variation of the input flux frequency ω_e. The graphs inside the systems of coordinates are theoretical predictions, panel a being an excerpt of panel b. The arrows indicate the experiments. The larger arrows correspond to the experiments evaluated in fig. 4. The numbers above the graphs and below the arrows are the theoretical and experimental oscillation periods, respectively, relative to the input flux period. C indicates chaos.

obtained, yielding more new windows, which because of their narrowness would be more difficult to find experimentally.

The arrows in fig. 1 indicate the experiments and the numbers beneath denote for the values of m (aperiodic oscillations are indicated by the letter C). In these experiments, we obtained the bifurcation from $m = 1$ to $m = 2$ at $\omega_e/\omega_0 \approx 1.5$, which is close to the numerically calculated value 1.4. The observed aperiodic region as well as the responses with $m = 7$ and $m = 5$ occur at somewhat larger frequencies than those predicted. Aperiodic oscillations between $m = 2$ and $m = 7$ or other periodic windows, which are expected from the theory, were not observed in this experimental series, probably because of the experimental difficulties in hitting the right interval. The transition from chaos to $m = 3$ is observed at $\omega_e/\omega_0 \approx 3$, the theoretically predicted value being $\omega_e/\omega_0 = 2.58$.

Examples of periodic behaviour of NADH as a

function of time for $m = 1, 2, 3$ and 5 are given in refs. 5 and 8. An example of a measured aperiodic response (at $\omega_e/\omega_0 = 2.76$) is shown in fig. 2. The lower part of this figure shows the periodic input flux, while the upper part shows a typical train of response oscillations having no recognizable period.

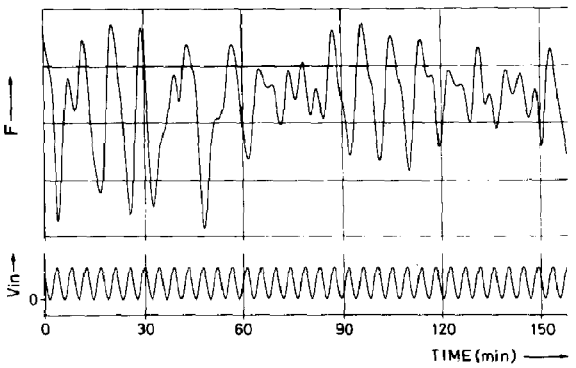

Fig. 2. Measured NADH fluorescence (upper curve) of yeast extract under sinusoidal glucose input flux (lower curve).

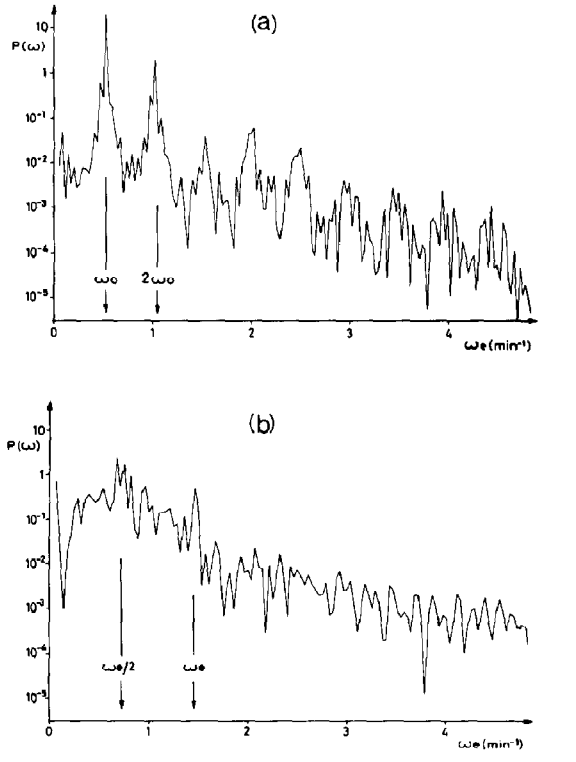

Fig. 3. Power spectrum of an oscillation at constant input flux (a) and a chaotic oscillation with $\omega_e = 2.76\ \omega_0$ (b). ω_0 is the system frequency at constant input flux and ω_e is the input flux frequency.

5.2. *Evaluation of experiments by different techniques*

5.2.1. *Determination of power spectra*

Fig. 3a shows the spectrum (see section 3.1) obtained for an oscillation resulting from a constant input flux. The highest peak corresponds to the oscillation frequency $\omega_0 = 2\pi/T_0$, where $T_0 = 12$ min. Also, several peaks representing higher harmonics can be seen. Fig. 3b shows the spectrum for the aperiodic oscillation shown in fig. 2 ($\omega_e = 2.76\ \omega_0$). Whereas fig. 3a consists of sharp peaks,

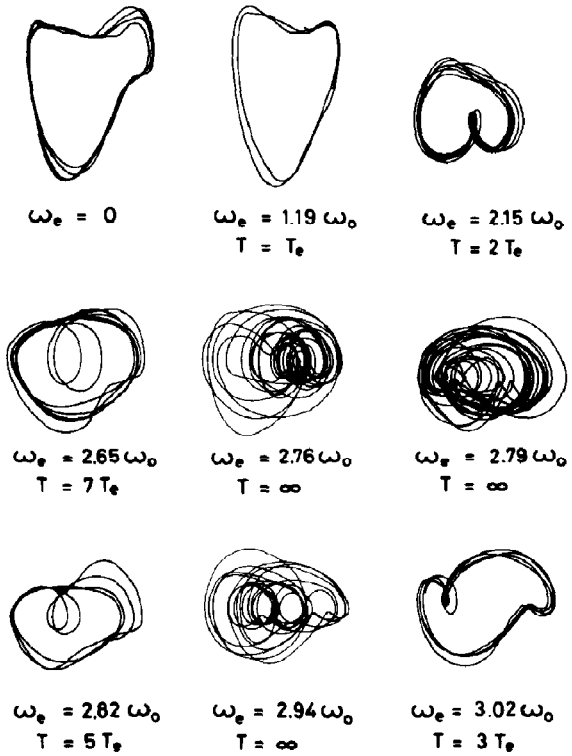

Fig. 4. Plots of dF/dt vs. F (F: measured NADH fluorescence in arbitrary units) for different values of the input flux frequency ω_e. ω_0 is the system frequency at constant input flux ($\omega_e = 0$). T and T_e are the response and input period, respectively.

fig. 3b is much closer to a continuous spectrum. Nevertheless, peaks at $\omega_e/2$ and ω_e can be discerned in fig. 3b. The highest peak, occurring at $\omega_e/2$, indicates that this aperiodic oscillation is related to entrainment by the 1/2-harmonic.

5.2.2. Determination of phase plane plots

Fig. 4 shows plots of dF/dT vs. F (see section 3.2) for constant input flux ($\omega_e = 0$) and for $m = 1$, 2, 7, 5, and 3, as well as for several aperiodic regimes. The different trajectories represent increasing ω_e/ω_0 and correspond to the larger arrows in fig. 1. Fig. 4 demonstrates the high sensitivity of the attractor shapes towards a change in the bifurcation parameter ω_e. Periodic responses are characterized by closed curves, except for small deviations due to the experimental error. The aperiodic trajectories (indicated by $T = \infty$) fill up an attracting region in an erratic way although some order can be discerned, resembling two-dimensional projections of strange attractors obtained in other areas of science, e.g., the solution of Duffing's equation [20] or the Lorenz attractor [21,22].

5.2.3. Determination of rotating phase planes

This evaluation method, described in section 3.3, is illustrated by examples in fig. 5. Fig. 5a shows the curve obtained for a periodic response

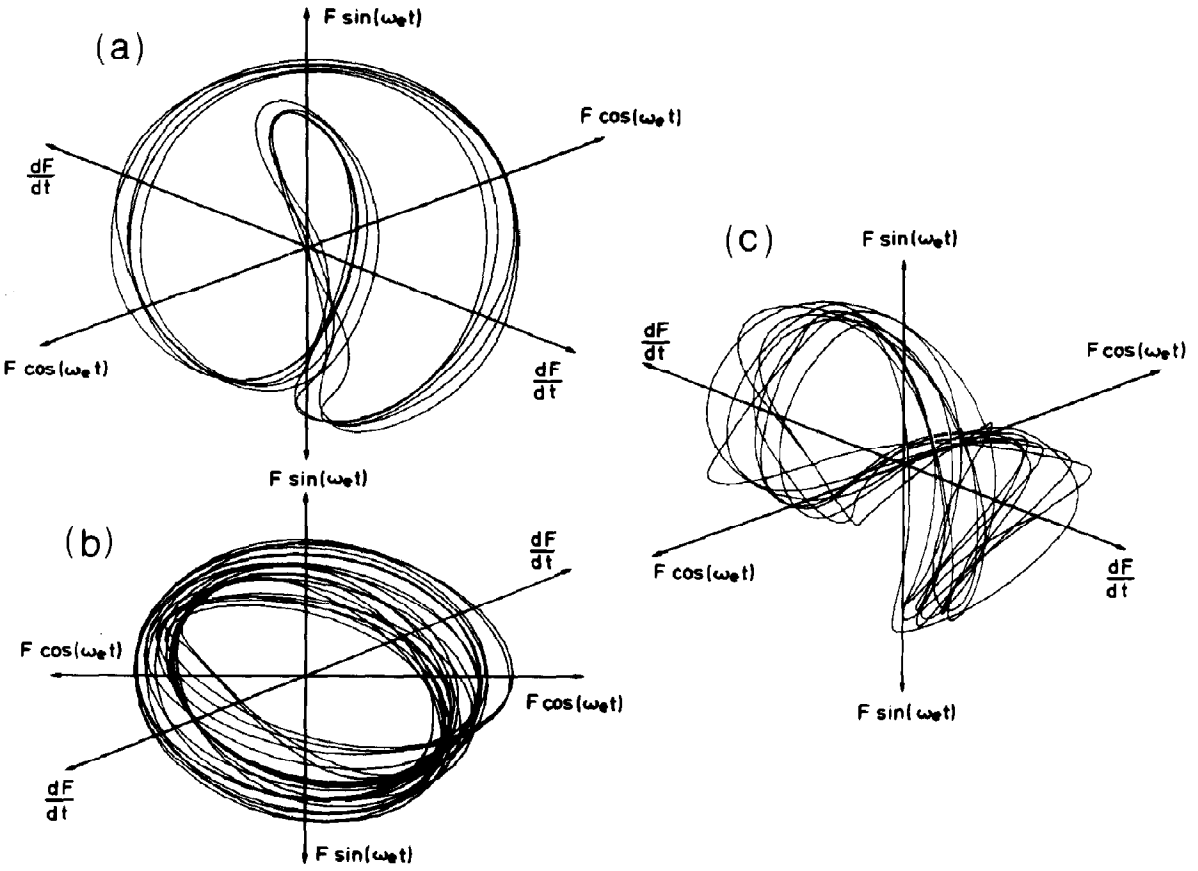

Fig. 5. Plot on the $dF/dt - F$ plane and rotation of this plane around the dF/dt axis with angular velocity ω_e (ω_e: input flux frequency) for a periodic response at $\omega_e = 2.15\ \omega_0$ (a), a chaotic response at $\omega_e = 2.76\ \omega_0$ (b) and a chaotic response at $\omega_e = 2.79\ \omega_0$ (c). The units are arbitrary and the axis starts from 0.

with period $2T_e$ (entrainment by the 1/2-harmonic) corresponding to fig. 4 at $\omega_e = 2.15\ \omega_0$. The trajectory is clearly closed with small fluctuations due to experimental error. Fig. 5b shows the curve obtained for the aperiodic regime corresponding to figs. 2 and 3b ($\omega_e = 2.76\ \omega_0$). The fluctuations here are much larger than those in fig. 5a, owing to the stochastic elements in deterministic chaos. In this plot, a toroidally shaped strange attractor is obtained. Fig. 5c shows the strange attractor resulting from a different input frequency (corresponding to $\omega_e = 2.79\ \omega_0$ in fig. 4), where we can discern a closed strip twisting in space. In comparison to the power spectra and the dF/dt–F analysis, it is now clearly seen that our experimentally obtained aperiodic oscillations obey deterministic rules.

5.2.4. Determination of stroboscopic plots on the phase plane

Evidence for the determinism underlying the observed aperiodic oscillations is furthermore strengthened by the stroboscopic dF/dt–F plots described in section 3.4 and exemplified in fig. 6. This figure was obtained for the same conditions as figs. 2, 3b, and 5b. The values of the phase φ are shown above the single plots in fig. 6 and each plotted point corresponds to one value of n in eq. 2. For a better visualization of the effect of varying φ, groups of points corresponding to a given set of values of n are linked together by straight lines for each phase in fig. 6. The linked groups of points indicated by α at the right of the picture for 0° moves downwards at 36°, then stretches mov-

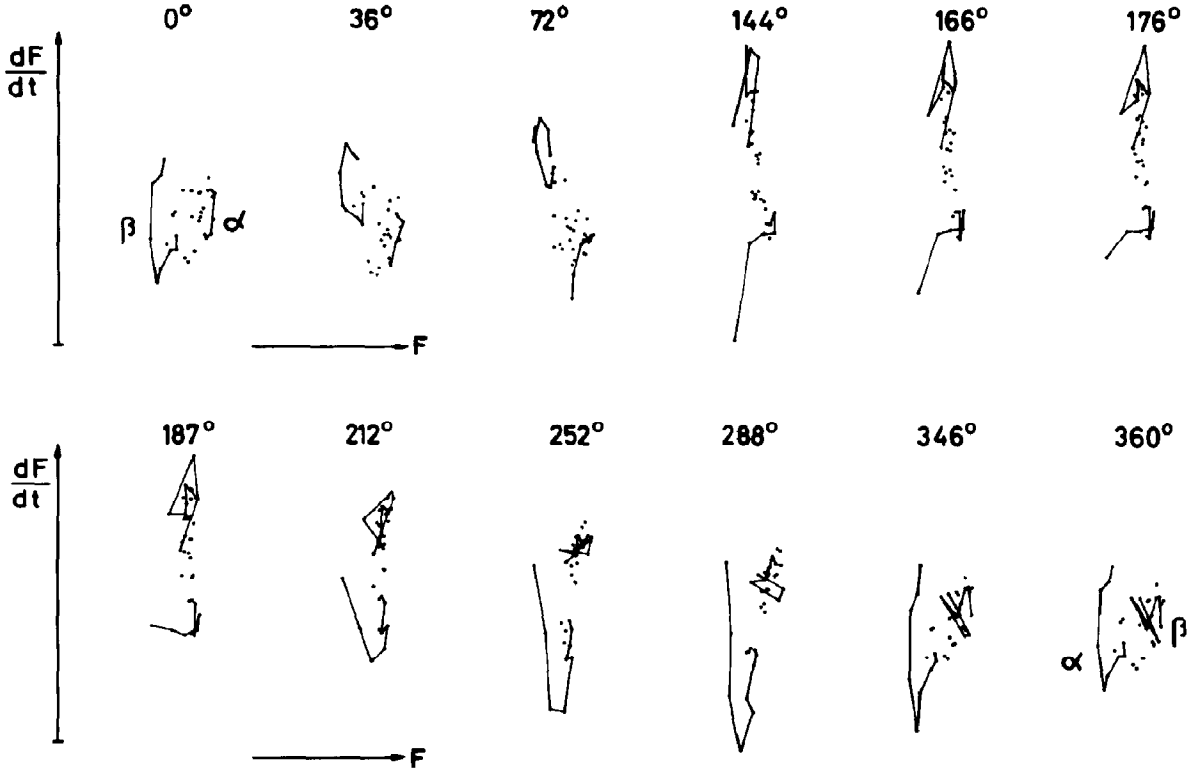

Fig. 6. Stroboscopic plot of dF/dt vs. F (F: measured NADH fluorescence in arbitrary units). The points are taken one input flux period apart at different input flux phase values. These phase values are given above the single plots. The straight lines connecting groups of points (α and β) permit visualization of a stretch-fold press process. The abscissa zero has been shifted from plot to plot.

ing further downwards between 72 and 144°, starts to fold upwards at 166° and continues folding and moving upwards until 360° = 0°. This group of points now appears at the left of the picture for 0°, as indicated by β. It moves upwards at 36° and gets pressed into the attractor until 360°. Thus. a stretch-fold-press process is completed after $\Delta\varphi = 2 \times 360°$, i.e., after a time interval $2T_e$. This aperiodic process is thus strongly related to an oscillation with a response period equal to $2T_e$ (entrainment by the 1/2-harmonic) as we have already noticed in the spectral analysis above (fig. 3b). The stretch-fold-press process is very similar to the baker's transformation (see ref. 23) and is a typical feature of strange attractors [24,25]. In particular, such transformation has been computed from data of voltage measurements in *Onchidium* giant neurons [26].

5.2.5. Determination of transfer functions

The method of stroboscopic transfer functions, described in section 3.5, is exemplified in fig. 7. Fig. 7a corresponds to an oscillation with response period equal to $3T_e$ (entrainment by the 1/3-harmonic) leading to three patches of points, as expected. Fig. 7b corresponds to the aperiodic oscillations shown in figs. 2, 3b, 5b and 6, permitting interpolation of a single-valued transfer function, shown by the continuous curve. This transfer function allows determination of a sequence of points having the same periodicity as fig. 7a, namely, three transfer processes as indicated by the numbers 1, 2 and 3. According to the Li-Yorke theorem [13], this transfer function thus admits chaos.

5.2.6. Determination of the Liapunov exponent by differentiation of the transfer function

The Liapunov characteristic exponent λ in the chaotic regime was determined using the transfer function given in fig. 7b. λ is given by eq. 3 and was estimated in the following way. For each measured transfer process, indicated by a plus sign in fig. 7b, we determined the slope of the interpolated transfer curve at the point on this curve closest to the plus sign. Then, we averaged the logarithms of the absolute values of the slopes. The result obtained in this way should certainly be only a rough approximation of the value given by eq. 3 because of experimental error and the finite

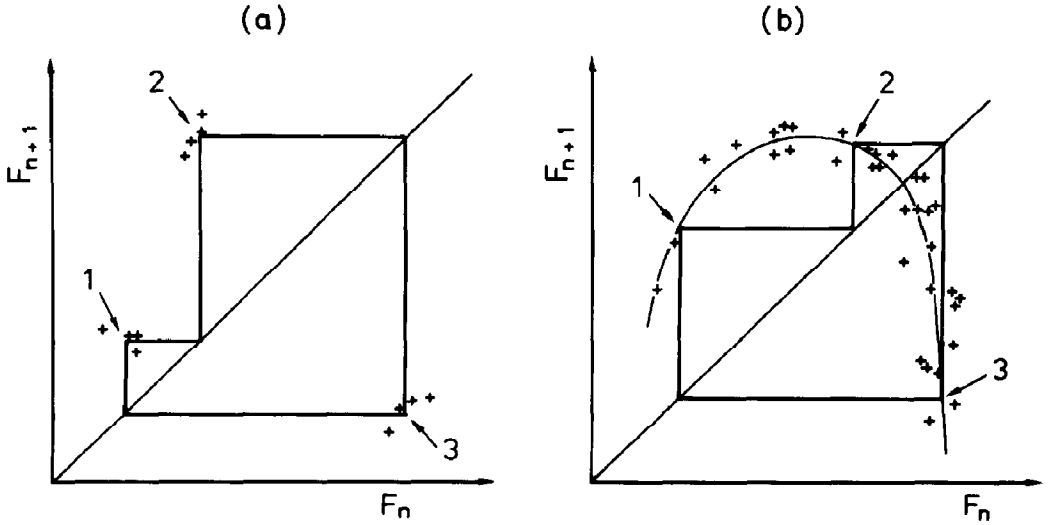

Fig. 7. Stroboscopic transfer function for a periodic response at $\omega_e = 3.02\ \omega_0$ (a) and for chaos at $\omega_e = 2.76\ \omega_0$ (b). The plus signs (+) indicate the signal F_{n+1} (arbitrary units) measured at time $(n+1)T_e$ vs. the signal F_n at time nT_e, where T_e is the input flux period. The solid curve in panel b is an interpolated transfer function. The period in panel a is $3T_e$ and the transfer function in panel b admits the same period. These periodicities are indicated in both panels by vertical and horizontal lines and by the numbers.

number of measured transfer processes. We obtained $\lambda \approx 0.93$. The positive sign of λ indicates that we are dealing with chaotic behaviour [6,14]. As mentioned in section 3.6, we can obtain the rate of information production by division of λ by the transfer time, which is $T_e = 4.4$ min here, yielding approx. 0.21 bits per min. Summarizing, it can be concluded from the diagnostic procedures that the observed aperiodic behaviour indeed results from a strange attractor giving rise to deterministic chaos in the cell-free glycolytic system.

6. Discussion

From the methodological point of view, the present work has shown that appropriate evaluation procedures can extract considerable knowledge from aperiodic measurements, which at first sight show no recognizable features. Spectral analysis shows that chaos has elements of both order, as demonstrated by peaks, and randomness, as indicated by high broad-band noise. However, this evaluation method has an averaging effect, yielding no information about the dynamics of the system.

In the plot of dF/dt vs. F, the elements of order and randomness become apparent through a visualization of the system dynamics. The order hidden in the aperiodic measurement becomes even more obvious with the introduction of the third dimension, as the dF/dt–F plane is rotated proportionally to time. Here, we visualize an attractor with a definite shape. It is noteworthy, that three dimensions are enough to characterize a system which is determined by a much higher number of metabolites. Such a reduction of dimensionality has also been reported for the Belousov-Zhabotinsky reaction [27]. The morphology of the strange attractor observed here comes to light in a detailed way with a stroboscopic plot of dF/dt vs. F, which reveals a foliation process similar to the baker's transformation. Further confirmation of the deterministic nature of the observed aperiodicities is obtained by the determination of a stroboscopic transfer function, where the 'order in chaos' is revealed by a single-valued bell-shaped curve. This curve fulfills the requirements given by Li and Yorke confirming the chaotic nature of the measurements. Finally, a differential analysis of this transfer function permits quantitatively labeling of the chaotic measurements by a single positive number with informational relevance, namely, the Liapunov characteristic exponent λ.

The Liapunov exponent is directly related to the rate of growth of information during a chaotic response. Chaotic systems can be considered as 'creative' in the sense of having a positive rate of increase of macroscopic information. Our estimated value for this rate, namely, 0.93 bits per transfer process, may be compared with that reported for the Lorenz attractor, which had been formulated with meteorological intentions [21,22], amounting to 0.98 bits per transfer process, where the transfer process is defined by a return of the trajectory through a cut transversal to the flow [14]. This is equivalent to our definition of a transfer process, if the measured oscillation is displayed by rotating the dF/dt–F plane with angular velocity ω_e and the resulting attractor is intersected by a half-plane defined by a given phase φ, as described in section 3. Upon division of the value 0.93 by the transfer time we obtain 0.21 bits/min, which lies within the range of values obtained theoretically in our previous work: 0–0.5 bits/min [6]. It has been conjectured that this quantity can be set equal to the rate of change of the Kolmogorov-Sinai entropy of the system [28,29]. A detailed discussion of informational aspects in chaotic dynamics is given in ref. 30. An alternative method reported recently for the computation of the maximum Liapunov characteristic exponent [31,32] is now being tested on our measurements, as will be discussed elsewhere.

We can summarize our result as follows. Evidence for chaos is obtained by application of Li-Yorke's theorem to the transfer plot and by the determination of a positive Liapunov exponent from the differentiated transfer plot. Evidence for determinism underlying the chaotic behaviour is obtained by the geometrical properties of the plots in dF/dt–$F\cos(\omega_e t)$–$F\sin(\omega_e t)$ space, the stroboscopic plots in dF/dt–F space and the stroboscopic transfer plot. The continuous plots of dF/dt vs. F, as well as the power spectra, give qualitative hints for the balance between order and chaos.

From the physiological point of view, the phenomena reported in the present work may have implications involving electrochemical membrane processes, since coupling of oscillating glycolysis and oscillating membrane potential has recently been reported for intact yeast [33,34]. In addition, it has been shown that membranes of *Onchidium* giant neurons [26] and *Nitella* [35] show responses towards periodic excitation similar to those reported here. Furthermore, in our previous theoretical works [6,7] we have pointed to the rich diversity of time patterns that a glycolytic system might display. These patterns undergo complex hysteresis loops when bifurcation parameters are changed, so that the system acts as a memory device where up to four time patterns may coexist for the same values of the bifurcation parameters ('tetrarhythmicity'). The coexisting patterns can be switched into one another by triggering the system with short additions or subtractions of substrates. In view of these facts, one may assume that the observations reported here are related to informational processes in neural networks.

As to the question of a possible biological role of chaos, diverging possibilities arise. On the one hand, chaos has been placed in connection with different kinds of arrhythmic disorders [36–38]. On the other, chaos may be the basis of trial-and-error adaptation mechanisms. The existence of some regulatory process controlling the avoidance or the incidence of chaos may be postulated. In view of the high sensitivity of the system towards bifurcation parameters, implying that very close parameter values lead to very different responses, a high precision is expected for this controlling process.

Acknowledgements

We would like to thank Mr. U. Heidecke and Mrs. I. Schlieker for their help in the laboratory, Mr. H. Schlüter for his assistance in the electronic set-up as well as Miss H. Kessel and Mr. H. Becher for programming assistance. We also thank Mrs. B. Plettenberg for efficient typing work.

References

1 B. Hess and A. Boiteux, in: Regulatory function of biological membranes, ed. J. Järnefelt (Elsevier, Amsterdam, 1968) p. 148.
2 B. Hess, A. Boiteux and J. Krüger, Adv. Enzyme Regul. 7 (1969) 149.
3 B. Hess and A. Boiteux, Hoppe-Seyler's Z. Physiol. Chem. 349 (1968) 1567.
4 L. von Klitzing and A. Betz, Arch. Mikrobiol. 71 (1970) 220.
5 A. Boiteux, A. Goldbeter and B. Hess, Proc. Natl. Acad. Sci. U.S.A. 72 (10) (1975) 3829.
6 B. Hess and M. Markus, in: Synergetics – from microscopic to macroscopic order, ed. F. Frehland (Springer Verlag, Berlin, 1984) p. 6.
7 M. Markus and B. Hess, Proc. Natl. Acad. Sci. U.S.A. 81 (1984) 4394.
8 M. Markus, D. Kuschmitz and B. Hess, FEBS Lett. 172 (1984) 235.
9 S. Blacher and J. Perdang, Physica 3D (1981) 512.
10 Harwell subroutine library, A catalogue of subroutines (Theoretical Physics Division, A.E.R.E., Harwell, 1973).
11 N. Packard, J. Crutchfield, D. Farmer and R. Shaw, Phys. Rev. Lett. 45 (1980) 712.
12 M. Kubiček and M. Marek, Computational methods in bifurcation theory and dissipative structures (Springer Verlag, New York, 1983).
13 T.Y. Li and J.A. Yorke, Am. Math. Mon. 82 (1975) 985.
14 R. Shaw, Z. Naturforsch. 36a (1981) 80.
15 V.I. Oseledec, Trans. Moscow Math. Soc. 19 (1968) 197.
16 D. Blangy, H. Buc and J. Monod, J. Mol. Biol. 31 (1968) 13.
17 A. Boiteux, M. Markus, T. Plesser, B. Hess and M. Malcovati, Biochem. J. 211 (1983) 631.
18 M. Markus, T. Plesser, A. Boiteux, B. Hess and M. Malcovati, Biochem. J. 189 (1980) 421.
19 M. Feigenbaum, J. Stat. Phys. 19 (1978) 25; J. Stat. Phys. 21 (1979) 669.
20 D.R. Hofstadter, Sci. Am. 245 (1981) 16.
21 E.N. Lorenz, J. Atmos. Sci. 20 (1963) 130.
22 C. Sparrow, The Lorenz equations: bifurcation, chaos and strange attractors (Springer Verlag, New York, 1982).
23 I. Prigogine, From being to becoming (Freeman, San Francisco, 1980).
24 E. Ott, Rev. Mod. Phys. 53 (1981) 655.
25 M. Sano and Y. Sawada, Phys. Lett. 97A (1983) 73.
26 H. Hayashi, S. Ishisuka, M. Ohta and K. Hirakawa, Phys. Lett. 88A (1982) 435.
27 J.C. Roux, R.H. Simoyi and H.L. Swinney, Physica 8D (1983) 257.
28 G. Benettin, L. Galgani and J.-M. Strelcyn, Phys. Rev. A14 (1976) 2338.
29 J.D. Farmer, Physica 4D (1982) 366.
30 J.S. Nicolis, G. Meyer-Kress and G. Haubs, Z. Naturforsch. 38a (1983) 1157.
31 A. Wolf and J. Swift, in: Statistical physics and chaos in fusion plasmas, eds. W. Horton and L. Reichl (Wiley, New York, 1984) p. 111.

32 A. Wolf, J.B. Swift, H.L. Swinney and A. Vastano, Physica D (1985) in the press.
33 B. Hess, A. Boiteux and D. Kuschmitz, in: Biological oxidations, eds. H. Sund and V. Ullrich (Springer Verlag, Berlin, 1983) p. 249.
34 B. Hess, D. Kuschmitz and M. Markus, in: Dynamics of biochemical systems, eds. J. Ricard and A. Cornish-Bowden (Plenum Press, New York, 1984) p. 213.
35 H. Hayashi, M. Nakao and K. Hirakawa, Phys. Lett. 88A (1982) 265.
36 M.C. Mackey and L. Glass, Science 197 (1977) 287.
37 L. Glass and M.C. Mackey, Ann. N.Y. Acad. Sci. 316 (1979) 214.
38 R. King, J.D. Barchas and B.A. Huberman, Proc. Natl. Acad. Sci. U.S.A. 81 (1984) 1244.